



Evidence of horizontal and vertical transport of water in the Southern Hemisphere Tropical Tropopause Layer (TTL) from high-resolution balloon observations

5 Sergey M. Khaykin¹, Jean-Pierre Pommereau¹, Emmanuel D. Riviere², Gerhard Held^{3*}, Felix Ploeger⁴, Melanie Ghysels^{2,a}, Nadir Amarouche², Jean-Paul. Vernier^{5,6}, Frank G. Wienhold⁷, Dmitry Ionov⁸

¹LATMOS, CNRS, Université de Versailles St Quentin, Guyancourt, France;

10 ²GSMA, Université de Reims Champagne Ardenne and CNRS, Reims, France;

³Instituto de Pesquisas Meteorológicas (IPMet), UNESP, Bauru, S.P., Brazil

⁴Forschungszentrum Jülich, IEK-7, Jülich, Germany;

⁵Science Systems and Applications, Inc, Hampton, Virginia, US;

⁶NASA Langley Research Center, Hampton, Virginia, US.

15 ⁷ETH Zurich, Institute for Atmospheric and Climate Science, Zurich, Switzerland;

⁸St.Petersburg State University, Russian Federation

^anow at: National Institute of Standards and Technology, Gaithersburg, MD, USA

*retired since 2014

20 *Correspondence to:* Sergey M. Khaykin (sergey.khaykin@latmos.ipsl.fr)

Abstract. High-resolution in situ balloon measurements of water vapour, aerosol, methane and temperature in the upper Tropical Tropopause Layer (TTL) and lower stratosphere are used to evaluate the processes controlling the stratospheric water budget: horizontal transport (in-mixing) and hydration by cross-tropopause overshooting updrafts. The obtained in situ evidences of these phenomena are analyzed using satellite observations by Aura MLS (Microwave Limb Sounder) and CALIPSO (Cloud-Aerosol Lidar and Infrared Pathfinder Satellite Observation) together with trajectory and transport modeling performed using CLaMS (Chemical Lagrangian Model of the Stratosphere) and HYSPLIT (HYbrid Single-Particle Lagrangian Integrated Trajectory) model.

30 Balloon soundings were conducted during March 2012 in Bauru, Brazil (22.3° S) in the frame of the TRO-Pico campaign for studying the impact of convective overshooting on the stratospheric water budget. The balloon payloads included two stratospheric hygrometers: FLASH-B (Fluorescence Lyman-Alpha Stratospheric Hygrometer for Balloon) and Pico-SDLA instrument as well as COBALD (Compact Optical Backscatter Aerosol Detector) sondes, complemented by Vaisala RS-92 radiosondes. Water vapour vertical profiles obtained independently by the two stratospheric hygrometers are in excellent agreement, ensuring credibility of the vertical structures observed.

35 A signature of in-mixing is inferred from a series of vertical profiles, showing coincident enhancements in water vapour and aerosol at the 425 K (18.5 km) level. Trajectory analysis unambiguously links these features to intrusions from the Southern Hemisphere extra-tropical stratosphere, containing more water and aerosol, as demonstrated by MLS and CALIPSO global observations. The in-mixing is successfully reproduced by CLaMS simulations, showing a relatively moist filament extending to 20 S°. A signature of local cross-tropopause transport of water is observed in a particular sounding, performed on a convective day and revealing water vapour enhancements of up to 0.6 ppmv as high as the 404 K (17.8 km) level. These are shown to originate from convective overshoots upwind detected by an S-band weather radar operating locally in Bauru.

45 The accurate in situ observations uncover two independent moisture pathways into the tropical lower stratosphere, whose manifestations are hardly detectable by space-borne sounders. We argue that the moistening by horizontal transport is limited by the weak meridional gradients of water, whereas the fast convective cross-tropopause transport, largely missed by global models, can have a substantial effect, at least at a regional scale.

1 Introduction

50 The Tropical Tropopause Layer (TTL) is a region of transition between tropospheric convective and stratospheric radiative regimes. Extending between the main level of convective outflow (12 - 14 km) and the maximum level reachable by convection (18 - 19 km), the TTL sets the boundary conditions for composition of air entering the global stratosphere (Fueglistaler et al., 2009). Accurate knowledge of the TTL physical processes and their interplay is thus of key importance for understanding climate change (Randel and Jensen, 2013). The role of stratospheric water vapour in global surface climate is now well recognized (Solomon et al., 2010; Dessler et al., 2013), evoking the necessity to better constrain the TTL processes governing the entry level of stratospheric water vapour.

55 There are two essential processes controlling the water vapour abundance in the TTL, thereby setting the global stratospheric water budget: (1) dehydration of air passing through the coldest regions of the TTL ("cold trap") via advection and slow ascent; (2) hydration by fast cross-tropopause vertical transport (convective overshooting). The dehydration occurs primarily in the Western Pacific – a region of large-scale slow ascent and cold TTL anomaly (Holton

60



and Gettelman, 2001), where the Cold Point Tropopause (CPT) temperatures experience minimum during austral summer (Gettelman and Forster, 2002).

65 While the dehydration (“freeze-drying”) process followed by upward and poleward transport of dry air is generally deemed to be of primary importance for the global stratospheric water budget, the effect of overshooting convection on the TTL water vapour (dehydration versus moistening) is under debate for many years (Randel and Jensen, 2013). There is a growing amount of observational evidence that overshooting convection, injecting material directly into the uppermost TTL has a moistening effect on the lower stratosphere (Kelly et al., 1993; Corti et al., 2008; Khaykin et al., 2009; de Reus et al., 2009; Schiller et al., 2009; Sargent et al., 2013). Consistent with the observations, simulations of overshooting events using cloud-resolving modeling show significant localized moistening of the lower stratosphere
70 (Chaboureau et al., 2007; Jensen et al., 2007; Grosvenor et al., 2007; Chemel et al., 2009; Liu et al., 2010). A dehydrating effect of overshooting may occur only if the TTL is initially supersaturated with respect to ice, as concluded by Jensen et al. (2007). In contrast to that, Randel et al. (2015) found that enhanced tropospheric convection within Asian and North American monsoons leads to reduced stratospheric water vapour. While upscaling the overshooting events and quantifying their net effect on water vapour remains a difficult task, various space-borne observations
75 suggest that the most vigorous convection, capable of direct transport of material into the lower stratosphere, is mostly restricted to the tropical land regions (Liu and Zipser, 2005; Ricaud et al., 2009; Iwasaki et al., 2010; Bergman et al., 2012; Khaykin et al., 2013a; Carminati et al., 2014).

Another important contributor to the composition of the TTL is the horizontal (isentropic) transport from the extra-tropical lower stratosphere (in-mixing), whose significance is pointed out in a number of model and observation based studies (Marcy et al., 2007; Konopka et al., 2009; Homan et al., 2010; Ploeger et al., 2012; Sargent et al., 2013). The in-mixing into the TTL is mostly driven by the anticyclonic circulation of the large monsoon systems in both hemispheres. The strongest Asian monsoon is considered responsible for the boreal summer maximum of in-mixing from the Northern Hemisphere (Konopka et al., 2009), whereas in the Southern Hemisphere, the in-mixing peaks in February (Ploeger et al., 2012). The net fraction of in-mixed air varies between 5% and 20% according to Ploeger et al., (2012) and appears
85 most apparent in tracers with stratospheric origins and strong latitudinal gradients, such as O₃ and HCl (Marcy et al., 2007).

Transport processes influencing the TTL composition, be that fast vertical (overshooting) or slower horizontal (in-mixing) transport have been mainly studied using trajectory and mesoscale modeling, whereas in situ observational evidence, indispensable to constrain the models, is lacking. Satellite observations, providing a global perspective, are not
90 capable of resolving kilometer scale vertical distribution of gases in the TTL, thus missing the signatures of transport processes.

This paper presents in situ observational evidence of the coexistence of the two transport mechanisms described above – convective overshooting and in-mixing detected by accurate high-resolution balloon-borne measurements of water vapour, methane and aerosol in the TTL above Bauru, Brazil (22° S) in March 2012. Satellite measurements, radar
95 acquisitions and trajectory/transport modeling are used to interpret the origin of vertical structures observed in situ. The paper is organized as follows: section 2 provides a description of experimental setup, instrumentation used and models exploited. Sections 3 and 4 describe the observations of horizontal and vertical transport signatures respectively. Section 5 discusses the relative importance of both transport mechanisms and summarizes the paper.

100 2 Experimental setup and instrumentation

A French funded project named TRO-Pico was aimed at characterizing the variability and frequency of convective water injections, their contribution at the regional wet season timescale, and improving the understanding of their role with respect to the cold trap at a wider scale. The project included two intensive balloon campaigns held in February-March 2012 and January-February 2013 under the auspices of the Brazilian Meteorological Research Institute IPMet – UNESP located in Bauru, São Paulo, Brazil (22.36°S, 49.03°W). The present study is based on the balloon experiments conducted during the first deployment in 2012, which included 7 flights of Raven Aerostrat zero pressure plastic balloons of 500 m³ and 1500 m³ and 6 flights of Totex 1200 g rubber balloons. The plastic balloon payloads
105 included Pico-SDLA instruments for water vapour and methane measurements whereas the rubber balloons were carrying lightweight FLASH-B and COBALD sondes for measurement of water vapour and aerosol backscatter respectively. The thermodynamical data were provided by Vaisala RS-92 radiosondes integrated in the payload.

An S-band weather radar of IPMet was continuously operating at the campaign site and provided information on the echo top heights. The IPMet radar has a 2° beam width and a range of 450 km for surveillance, but when operated in volume-scan mode every 7.5 minutes it is limited to 240 km, with a radial resolution of 250 m and 1° in azimuth, recording reflectivities, spectral width and radial velocities at 16 elevations between 0.3° and 45°.
115

On 13 March 2012, a rubber balloon payload (FLASH-B + COBALD) was flown in parallel with a plastic balloon payload (Pico-SDLA H₂O), which provided quasi-simultaneous measurements of water vapour by two hygrometers. Point-by-point intercomparison of the obtained water vapour profiles (Ghysels et al., 2016) showed excellent agreement with a mean difference above 15 km of 0.5% (0.02±0.21 ppmv).
120



2.1 Balloon-borne instruments

125

Fluorescence Lyman-Alpha Stratospheric Hygrometer for Balloon (FLASH-B) is a compact lightweight sonde developed at the Central Aerological Observatory of Roshydromet, Russia for water vapour measurements in the upper troposphere and stratosphere (Yushkov et al., 1998). The instrument uses an open coaxial optical layout, where the analyzed volume is located outside the instrument. This allows reducing the size of the instrument to a small sonde with a total weight of about 1 kg including batteries but restricts its application to night time. The typical precision of the hygrometer in the stratosphere is 5–6 %, whereas the total uncertainty, including the calibration error is estimated to be below 10 %. This estimate is rather conservative as suggested by comparisons against other water vapour instruments, showing discrepancies below 5 % (Khaykin et al., 2013b). Here we use the data averaged over 4 s, resulting in a vertical resolution of 20 m during ascent and 50 m during the parachuted descent in the lower stratosphere. The detection limit is 0.1 ppmv. The flight configuration of FLASH-B, in which the analyzed volume is located beneath the downward-looking optics, causes self-contamination due to water outgassing from the instrument and eddy diffusion above about 70 hPa during ascent when the contribution of water residing on the instrument walls becomes comparable to the ambient vapour pressure. By contrast, the descent measurements at the bottom of the flight train in undisturbed air are contamination-free throughout the stratosphere (Khaykin et al., 2013b).

130

135

140

Pico-SDLA H₂O and CH₄ are lightweight infrared spectrometers measuring in-situ water vapor at 2.63 μm and methane at 3.24 μm respectively by direct absorption spectroscopy (Durry et al., 2008; Ghysels et al., 2011). The optical path length for water vapor and methane measurements are 1 m and 3.6 m respectively in ambient air. During the campaign the mass of these spectrometers with the electronic parts and the mechanical protections was less than 9 kg (Pico-SDLA H₂O) and around 15 kg (Pico-SDLA CH₄). The uncertainty of the measurements is defined by the signal-to-noise ratio of the spectra, the polynomial order for baseline fitting, the number of points chosen for the interpolation, the quality of the spectroscopic parameters and the temperature and pressure measurements accuracy. The total uncertainty of water vapor measurements ranges from 7.5 % to 3.5 % in the TTL. The total uncertainty of methane measurements ranges from 3.5 % to 5 % between 15 km and 22 km (Ghysels et al., 2014).

145

150

Compact Optical Backscatter Aerosol Detector (COBALD) is a compact balloon-borne backscatter instrument developed in the group of Prof. Thomas Peter at ETH Zurich. With a total weight of approximately 550 g including batteries, COBALD measures molecular, aerosol and cloud particle backscatter in the atmosphere from the ground to the level of balloon burst. COBALD sondes have been applied for studies of cirrus clouds (Brabec et al., 2012; Crisan et al., 2014) volcanic aerosol (Bukowiecki et al., 2011) and non-volcanic aerosol (Vernier et al., 2015). The instrument makes use of two LEDs of 250mW optical power each emitting light at 455 and 940 nm wavelengths. To register the backscattered light, a silicone photodiode is placed between the LEDs, and the associated optics establishes an overlap region at distances larger than 0.5 m in front of the instrument. The instrument is designed for night-time use only, as solar radiation saturates the detector. Radiosonde pressure and temperature are used to calculate the molecular backscatter, which is then used to infer the Scattering Ratio (SR) as total signal referenced to molecular contribution. The SR profiles are binned to 1 hPa pressure intervals to reduce measurement noise, which typically increases in the stratosphere. While the SR is not quantified absolutely, the analysis of the entire sounding profile leads to an absolute error interval of 5% with precision better than 1% in the lower stratosphere (Vernier et al., 2015). By definition, the aerosol contribution to the SR (aerosol scattering ratio) is given as a surplus with respect to unity, i.e. SR – 1.

155

160

2.2 Space-borne observations

165

The Microwave Limb Sounder (MLS) instrument, launched in 2004 onboard the Aura satellite, is designed to measure a number of chemical species and temperature and provides over 3500 vertical profiles per day evenly distributed between 82° S to 82° N. Here we use the version 4.2 water vapour profiles described by Livesey et al. (2015), who report for the lower-middle stratosphere a vertical resolution of 2.8 – 3.2 km, a horizontal resolution of 198–290 km, an accuracy of 4–9% and a precision of 6–15 %. The data screening criteria specified by Livesey et al. (2015) have been applied to the data.

170

Cloud-Aerosol Lidar with Orthogonal Polarization (CALIOP) is a primary instrument onboard the CALIPSO satellite, operational since 2006 (Winker et al., 2009) and providing backscatter coefficients at 532 and 1064 nm. The vertical resolution of CALIOP varies with altitude – from 30m in the lower troposphere, to 180m in the stratosphere. In this study we use the CALIOP night-time 532 nm level 1B version 4.0 product for computing zonal-mean scattering ratios after discarding the South Atlantic magnetic anomaly zone. The data are post-processed using a treatment described by Vernier et al. (2009) and cloud-cleared in the upper troposphere using a depolarization ratio threshold of 5%.

175

2.3 Trajectory and transport modeling

180

For tracking the origin of air masses sampled in situ by the balloons, we use the models HYSPLIT and CLaMS. HYSPLIT (HYbrid Single-Particle Lagrangian Integrated Trajectory) model (Stein et al., 2015) was initialized by GDAS (Global Data Assimilation System) reanalysis provided at 0.5° x 0.5° grid and 55 sigma- pressure levels between the surface and 10 hPa. The trajectories are calculated using altitude as the vertical coordinate, with the vertical velocity deduced from the GDAS meteorological fields. CLaMS (Chemical Lagrangian Model of the Stratosphere) is a modular

185



190 Chemistry Transport Model (CTM) developed at Forschungszentrum Jülich, Germany (McKenna et al., 2002). The model transport is driven by the meteorological fields from the European Centre for Medium-range Weather Forecasts (ECMWF) ERA-Interim reanalysis (Dee et al., 2011). The trajectories are calculated using potential temperature as the vertical coordinate, with the (diabatic) vertical velocity deduced from the forecast total diabatic heating rate. Small-scale atmospheric mixing is parameterized in the Lagrangian model CLaMS in relation to shear and strain rates in the large-scale flow, such that the mixing occurs in regions of strong flow deformations. Further details about CLaMS simulation used here are given by Pommrich et al. (2014).

195 3 Evidence of horizontal transport (in-mixing)

3.1 Detection of in-mixing signatures

200 Five balloon measurements of water vapour (FLASH-B and Pico-SDLA) and aerosol (COBALD) conducted over a period between 11 and 16 March 2012, revealed a recurring 300 – 500 m thick layer of enhanced water vapour and aerosol concentration centered at the 425 K potential temperature level (~18.5 km). The amplitude of enhancements was reaching 15% (0.5 ppmv) in water vapour mixing ratio and 29% in aerosol scattering ratio. A methane vertical profile obtained by the Pico-SDLA instrument on 14 March revealed a reduction of CH₄ mixing ratio by 100 ppbv (~ 6%) at the same level. Figure 1 displays the vertical profiles of water vapour and scattering ratio obtained on 13 March, when the layer had the largest thickness and amplitude of enhancement. The methane profile obtained on 14 March, featuring a local minimum in the corresponding layer, is also displayed in Fig.1. Note that the altitude and amplitude of the water vapour enhancement are identical to those reported by the Pico-SDLA hygrometer (see Sect. 2 and Ghysels et al., (2016)). Two other local maxima in water vapour, detected by FLASH-B at 404 K and 386 K, do not have corresponding enhancements in SR and are not observed in other flights. These features are discussed in Section 4. The nearest matching MLS water vapour profile, acquired on the same night ~50 km away from the sounding location is also provided in Fig. 1. It demonstrates a good agreement with the coincident balloon measurements, although the sub-kilometer vertical structures are expectedly missed by MLS.

210 COBALD backscatter measurements were converted to 532 nm for comparison with CALIPSO after deduction of the Angstrom exponent from 455 nm and 940 nm COBALD channels, similarly to Vernier et al. (2015). The zonally and monthly averaged SR profile from CALIPSO, showing a step-like increase in scattering ratio just above the upper boundary of TTL, is consistent with COBALD profile, however the enhancement at 425 K is only seen in COBALD local observation. This suggests a limited spatiotemporal extent of the observed feature.

220 3.2 Satellite perspective and trajectory modeling

The origin of the observed layer is investigated using CLaMS trajectories initialized at 8 levels within and around the layer – these levels are marked by circles and triangles respectively in Fig. 1. The same convention for markers is used in Fig. 2, displaying the latitudinal locations of the air masses from within and outside the layer 15 days prior to the 13 March sounding. Trajectory analysis suggests that the water/aerosol-enriched layer originates from the extra-tropical stratospheric overworld ($\theta > 380$ K), as opposed to the layers directly below and above, which are traced back from within the Southern hemisphere tropics. The transport from mid- and high latitudes is of quasi-isentropic nature as the isentropes shown in Fig. 2 suggest.

225 The latitude-altitude distribution of water vapour from MLS displayed in Fig. 2 explains the enhanced humidity of the layer: the extra-tropical stratosphere around the 440 K level contains about 20% more water than the tropical lower stratosphere. Indeed, the mixing ratio of 4.2 ppmv measured in situ within the layer is fully compatible with MLS zonal-mean values at the source locations. The same interpretation is applicable to the enhanced aerosol in situ readings in the layer: higher aerosol load (SR > 1.07) of the Southern mid-latitude stratosphere is evident.

230 The water vapour minimum throughout the TTL, as seen by MLS in February, is associated with dehydration of air parcels advected through the “cold trap” predominantly above the Western Pacific region (Holton and Gettelman, 2001). The increase of LS water towards high latitudes is commonly associated with the diabatic subsidence of air - enriched with water through methane oxidation - in the descending branch of Brewer-Dobson circulation. The latitude distribution of aerosol load, featuring a minimum in the TTL and mid-latitude lowermost stratosphere, can be explained by cross-tropopause transport of clean tropospheric air (cleansing) during the austral summer convective season (Vernier et al., 2011).

240 3.3 CLaMS transport simulation

245 The in-mixing of extra-tropical air - as suggested by the trajectory analysis - is precisely demonstrated by the water vapour fields simulated by CLaMS. Fig. 3a displays the CLaMS water vapour at 420 K above South America and Southern Atlantic ocean. The simulation reports water mixing ratios below 3 ppmv wherever the winds are easterly, that is mainly within the tropical belt, where water vapour is depleted by “cold trap” dehydration. South of 40°S, strong westerly winds and higher mixing ratios (>4 ppmv) prevail. The ERA-int wind fields in Fig. 3 show an enhanced meridional wind component above the Southern Atlantic, which supplies humid high-latitude air up to 40° S, where it is



250 entrained by the tropical zonal flow. As a result, a moist filament, several thousands kilometers long and only a few hundreds kilometers thick is formed. The filament extends sharply above the sounding location on 13 March.

255 Over the following days, as suggested by the model simulations (not shown), the filament weakens, mixes-out with the ambient drier air and vanishes completely by 17 August. According to CLaMS, the intrusion was most prominent on 13 March, which is fully compatible with the balloon soundings that showed a maximum amplitude of water enhancement at 420-430 K on 13 March. Simulation of methane fields (Fig. 3b) at this level reveals corresponding filament of methane-poor air, which is compatible with the in situ methane profile of 14 March, showing a subtle reduction of methane mixing ratio at the 425 K level. The age of air inside the filament – as estimated using CLaMS – is 18 months on average, which is substantially older than the tropical belt air, with mean age of about 7-8 months.

260 4 Evidence of vertical transport of water (overshooting)

In the previous section we showed that the enhancements in water vapour and aerosol at 425 ± 5 K, detected in a series of successive soundings and corresponding to methane reduction feature can be unambiguously attributed to long-range horizontal transport (in-mixing). However, this interpretation does not hold for the two other water vapour enhancements at 404 K and 386 K - specific to a single sounding, which prompts to seek for another origin of these features.

265 4.1 Hydration signatures

270 Fig. 4 displays water vapour and temperature profiles obtained by Pico-SDLA (balloon descent) and FLASH-B (ascent and descent) successively in time in the quasi-simultaneous soundings of 13 March. The levels of interest, at which the FLASH-B descent profile showed sharp enhancements, are marked by dashed lines with indication of time when these levels were sampled. The FLASH-B ascent profile is limited to below 18.7 km as the measurements above that level are affected by water outgassing, which introduces a positive bias (with respect to the clean descent measurement) increasing with altitude (Sect. 2.1).

275 The Pico-SDLA descent profile (Fig. 4a) shows a 240 m thick humid layer centered at 404 K (17.8 km, 82 hPa, 22:06 UT) with amplitude of enhancement of 0.6 ppmv. The amplitude is estimated as a difference between the peak value of the enhancement and a mean value over the underlying and overlying 300 m thick layers. In the ascent profile of FLASH-B (Fig. 4b), the enhancement at 404 K is discernible, however its amplitude (~ 0.2 ppmv) is close to the detection limit of the instrument (0.1 ppmv). The descent profile of FLASH-B (Fig. 4c) reveals two sharp enhancements, both around 200 m thick: at 404 K (0.5 ppmv) and a smaller one (0.4 ppmv) at 386 K (17.1 km, 93 hPa, 23:46 UT). The lower layer has a lesser amplitude of enhancement (0.2 ppmv) in the FLASH-B ascent profile and is barely discernible in the Pico-SDLA descent profile. Note that given the balloon flight trajectories, the horizontal distance between the detections of humid layers by Pico-SDLA and FLASH-B does not exceed 30 km and 100 minutes, whereas FLASH-B ascent and descent measurements at 17-18 km altitude are only 10 km and 30 minutes apart.

285 Notable variability of water vapour vertical structure on a scale of a few tens of kilometers (minutes) prompts to local processes such as overshooting convection, capable of injecting water above the tropopause. Throughout the paper we refer to the term “overshooting” with regard to the mass transport across the Lapse Rate Tropopause (LRT). The LRT altitude on 13 March inferred from the FLASH-B sounding (RS-92) amounted to 16.4 km.

290 4.2 Convective activity on 13 March

An extremely weak pressure gradient over Southeast Brazil, combined with the equally weak upper air circulation, provided an ideal situation for convective activity over the State of São Paulo on 13 March. Isolated thunderstorms first developed in the southeast sector of the IPMet radar around noon Local Time (LT=UT-3h), but quickly consolidated into large multi-cellular complexes, with several cells overshooting into the lower stratosphere during the later afternoon. A sequence of radar echo top images (240 km range, reflectivity threshold 10 dBZ) between 10 and 15 h UT, acquired every 7.5 minutes, revealed over 10 different convective cells reaching above 17 km.

300 Shown in Fig. 5 is a composite radar image including all echo tops reaching above 15-17 km (see Sect. 4.4 for interpretation of the echo top altitudes) detected by the radar on 13 March in the upwind quadrant of the soundings. Whereas the convective cloud systems hosting the overshooting cells extended for over 100 km, the areas of radar echoes above 17 km were limited to a few tens of kilometers or less in diameter. The lifetime of overshooting cells, emerging sporadically above the “mother cloud”, was typically limited to 2 successive radar volume scans, i.e. 15-29 minutes.

305 Given the position of the overshooting cells relative to the balloon soundings and the weak wind velocity in the TTL (< 5 m/s), one can assume that the cells closest to Bauru (e.g., those marked by black arrows in Fig. 6) are more likely to affect the composition of air sampled by the balloons.

310 Figure 6 displays the temporally-resolved cumulative area of all overshooting cloud tops observed on 13 March within the quantitative detection range of the IPMet radar (240 km). Remarkable is the peak of overshooting area around 17 h local time, which is consistent with a typical diurnal cycle of convection above land (Liu and Zipser, 2005). The maximum convective activity was recorded at 17:30 local time (14:30 UTC), when the total area of cloud tops above 17 km and 16 km reached 100 km² and 200 km² respectively. For comparison, the combined overshooting area of the two



small cells closest to Bauru (marked by arrows in Fig. 5 and by stars in Fig. 6) constitutes only about 4% of the daily maximum of total cloud area above 16 km.

315 4.3 Overshoot tracking

The overshooting cells potentially responsible for the water enhancements were identified using HYSPLIT backward trajectories (not shown) and a sequence of radar echo top images. The hydrated air parcels sampled at 404 K and 386 K were traced backward in time, through the radar scans sequence, until a parcel's trajectory matched in space and time with a convective cell reaching above 16 km. Two different convective cells, occurring at 16:46 UT, "cell 1" and 17:38 UT, "cell 2" (marked by black arrows in Fig. 5), whose overshooting tops were located 45 km and 32 km respectively, upwind from the FLASH-B sampling location (49 km and 37 km from Pico-SDLA), were identified for both hydrated layers. It should be noted that the trajectory calculations strongly depend on the accuracy of the wind fields in the meteorological data fed into the model. This becomes particularly important when the tracked target (overshooting cell in this case) is smaller than a grid cell of meteorological data field. We attempt to compensate for this uncertainty by computing an ensemble of trajectories to estimate the dispersion of air parcels affected by overshooting convection.

Figure 7 shows two blowups of the radar echo top images, where the overshooting cells, presumably responsible for the hydrated layers, are outlined with black rectangles. Superimposed on each radar image is an ensemble of 144 forward trajectories initialized within the rectangles at 4 levels corresponding to the hydrated layers vertical extent and spaced vertically by 50 m. The trajectory ensembles, color-coded by UT, show the spatiotemporal evolution of the plumes of overshooting cells. Note that the altitude excursions of the air parcels did not exceed 200 m according to HYSPLIT simulations. The locations, where the hydrated layers were sampled are marked with circles along FLASH-B and Pico-SDLA balloon flight trajectories.

The Cell 2, linked by trajectories with the hydrated layer at 404 K (Fig. 7b) had a lifetime of two radar scans and a diameter of less than 10 km. Its plume, as suggested by the trajectory ensemble, has reached the sounding locations by 22 h UT and covered all three sampling locations where the hydrated layers were detected. The FLASH-B ascent sampling at 23:15 UT is located on the edge of the "plume", which may explain the subtlety of the corresponding water vapour enhancement (Fig. 4b). The Cell 1, linked with the hydrated layer at 386 K (Fig. 7a), had yet smaller size and a lifetime limited to a single radar scan. Its plume had a smaller dispersion and covered the FLASH-B sampling locations only, which is likely the reason why the hydrated layer at 386 K was not unambiguously detected by Pico-SDLA (Fig. 4a).

Overall, the above analysis suggests the relation between the hydrated layers and convective overshoots upwind, occurring 5-6 hours before the soundings. The question is - could any other overshooting cells in the upwind area be responsible for the hydrated layers? As can be seen in Fig. 5, the overshooting cells at 16:46 UT and 17:38 UT are remarkably smaller than the other ones occurring upwind on that day, however the ERA-int wind velocities in the 100-70 hPa layer (shown as white vectors in Fig. 5) of the order of 5 m/s or less would not allow more distant overshoots to be transported in time to the sounding location. For example, the plumes of two larger cells detected south of Botucatu (Fig. 5), would have reached the sounding locations several hours after the time of measurements. On the previous day (12 March) a medium-sized overshooting cell was detected about 200 km southeast of Bauru at 14:16 UT (not shown), however its location and timing do not allow to link it with the sounding location using trajectories. Therefore we are led to conclude that the two small overshooting cells of 13 March, closest to the measurement location, are the most likely sources of the hydrated layers.

355 4.4 Overshooting top altitude

The two overshooting cells shown in Fig. 7 are characterized by extremely strong updrafts, facilitating their rapid vertical growth. Figure 8 shows Cell 1 and Cell 2 vertical cross-sections, highlighting the complexity of the cells' structures and air flow. The vertical cuts were made along the base lines A-B and C-D (shown in Fig. 7a and 7b respectively) using a reflectivity threshold of -6 dBZ (cf. 10 dBZ in Fig. 5 and 7) to enhance the sensitivity in the near range (the -2 dBZ contour is visible up to a range of 40 km). The maximum reflectivity was 52,8 dBZ and 54,2 dBZ in Cell 1 and Cell 2, respectively, typical for severe tropical storms, likely to produce hail on the ground.

The maximum height of the radar echo top for Cell 1 and 2 was 17.1 km and 17.3 km respectively as can be inferred from Fig. 8. While this is consistent with the altitude of the corresponding moist layers, it is important to point out that radar can only detect rain drops, whereas the actual top of the cloud is likely to extend significantly higher, where ice crystals are the only hydrometeors in the overshooting turret, but which cannot be detected by the S-band radar.

The radial velocity cross-sections for both cells (not shown) obtained using the IPMet radar's Doppler facility suggest that the outflow from both cells into their anvils exceeded -13 m/s. Considering the ambient flow field of about 3 m/s in the same direction, the true outflow velocity can be estimated at about 10 m/s. The Cell 1 translation was only 2.7 - 4 m/s towards northeast, but would contribute to re-direct the moisture flux towards the balloon trajectories. Similar results are obtained for the Cell 2.

4.5 Hydration process



375

The overshooting hydration is commonly conceived as a two-stage process: geyser-like injection of adiabatically cooled air (Danielsen, 1993; Jensen et al., 2007) together with ice particles (Nielsen et al., 2007; Corti et al., 2008) that further sediment out and/or sublimate, thereby increasing locally the water vapour amount at the level of detrainment (Khaykin et al., 2009; Schiller et al., 2009). Cooling signatures corresponding to the hydrated layer at 404 K can be seen in Fig. 4, however the backscatter measurements during that flight (Fig. 1) do not provide any indication for the presence of ice particles in the hydrated layers. Apparently, the ice detrained from convective updrafts has fully sublimated before the plume was sampled. Indeed, the minimum saturation mixing ratio in the TTL – as derived from radiosonde data from the FLASH-B flight – amounted to 8.5 ppmv at 404 K (which translates into 46 % relative humidity over ice, RH_i) implying that the air was far from saturation conditions.

380

385

390

The observation of overshooting hydration presented here can be compared to a similar case captured by a balloon sounding conducted during monsoon season in West Africa (Khaykin et al., 2009). However, in that case a water vapour enhancement of 1.1 ppmv was observed together with a layer of ice particles in subsaturated air (56% RH_i) above a cloud anvil, at 392 K (17.6 km altitude), indicating the ongoing sublimation of ice. A small cooling signature and a dip in ozone within the moist layer were also observed. The analysis of local radar acquisitions in Africa suggested that the ice was injected by a nearby upwind overshooting cell, 30-60 minutes before the detection – a much shorter time interval than that (5 – 6 h) in the present case.

5 Discussion and summary

395

High-resolution balloon-borne measurements of water vapour and aerosol reported here provide insights into the processes controlling the composition and structure of the TTL. The credibility of water vapour measurements exploited is confirmed by the excellent agreement between FLASH-B and Pico-SDLA hygrometers (Ghysels et al., 2016), capturing identical vertical structures. The analysis provided above links the observed fine structures of TTL water vapour with two independent and concurrent transport processes – in-mixing from the extra-tropical stratosphere and convective hydration – both reflected by local enhancements of water vapour mixing ratio of similar amplitude. Remarkably, the signatures of both transport pathways, vertically spaced by only a few hundreds of meters, were coexisting in the same balloon profile.

400

410

The interpretation of the observed structures and their attribution to different transport pathways into the TTL was based on the use of satellite and ground-based radar observations together with back trajectories and transport modeling. CLaMS simulation precisely reproduces the signature of in-mixing from the extra-tropical LS, reflected in the measurements as coincident water vapour enhancement and methane depletion at 420-430 K. Both vertical and temporal extents of the observed features are fully consistent with those suggested by CLaMS simulation, revealing an intrusion of water-rich and methane-poor air within an elongated filament. The coincident local maximum of scattering ratio was interpreted using CALIPSO observations, showing larger aerosol load in the extra-tropical LS compared to the clean TTL. Although coincident enhancements in water vapour and aerosol can be in principle interpreted as a result of convective injection of ice particles and their partial sublimation, the argumentation provided above strongly supports the idea of horizontal in-mixing as being the cause.

415

420

The effect of in-mixing on the TTL composition and its seasonality is known to be most apparent in tracers of stratospheric origin and with strong meridional gradients in the lower stratosphere (Ploeger et al., 2012). Indeed, in-mixing was found to contribute considerably to the annual cycle of ozone above the tropical tropopause (Konopka et al., 2009; 2010). At the same time, the effect of in-mixing on the TTL water vapour seasonality is expected to be small at the tropics-wide scale (Ploeger et al., 2012). The in situ evidence of water vapour enhancement of 15% in a 500 m thick layer due to in-mixing – as reported in this study - can neither dispute nor support the above inference. Hence, we can only conclude that the intrusion of mid-latitude air (containing slightly more water and slightly less methane) into the uppermost TTL predicted by CLaMS is fully confirmed by the measurements provided here. We note also that the manifestation of this transport pathway in water vapour and methane has never been previously evidenced by observations.

425

A less expected phenomenon evidenced by our observations is the effect of in-mixing on aerosol content of the TTL in the absence of volcanic eruptions injecting sulphur into the stratosphere. While a local maximum of aerosol SR at lower stratospheric levels is a typical signature of volcanic plume, in our case it is conditioned by a higher stratospheric background aerosol load at mid-latitudes with respect to the clean TTL in March, that is after the austral summer convective season, when systematic injections of clean tropospheric air reduce the aerosol abundance throughout the TTL (Vernier et al., 2011).

430

435

The fast cross-tropopause transport of clean air by overshooting has been shown to have a global-scale effect on the stratospheric aerosol budget (Vernier et al., 2011). Regional effects of overshooting have been detected in various tropospheric tracers, such as N₂O, CH₄ and CO (Ricaud et al., 2007; 2009). Carminati et al. (2014) used MLS daytime and nighttime observations to investigate the diurnal cycle of water vapour, cloud ice-water and temperature. They found a daytime moistening of the TTL and LS (up to 6%) over southern tropical land during austral summer, which was attributed to convective hydration. According to Iwasaki et al. (2010), the total number of overshoots penetrating the 380K level across the tropical belt is 7×10^6 per year as inferred from CALIPSO and CloudSat radar observations. A hydration of about 100 t per event was estimated from these data. The frequency of clouds above 390 K was estimated to



be 5-10 % by Massie et al. (2010) using High Resolution Dynamic Limb Sounder (HIRDLS) and CALIPSO observations.

440 It should be noted that MLS, CALIPSO, CloudSat and HIRDLS, all operating within the A-TRAIN constellation, sample only local times around 01:30 and 13:30, and therefore miss the strong late-afternoon peak of convective activity above tropical continents. Another important factor, hindering observation of convective moistening, is the broad vertical resolution of MLS profiles, which totally miss the hydration signatures manifesting themselves at sub-kilometer vertical extent. On the modeling side, CTM simulations (like the one reported here), being capable of capturing fine structures due to horizontal transport, do not reproduce the overshooting hydration signatures, originating from isolated convective systems. Presently, the localized deep convection and its impact on TTL composition and temperature can 445 only be reliably simulated using non-hydrostatic cloud resolving models. Extrapolation of these results to regional or global scale remains a great challenge, partly due to the lack of observational constraints (Randel and Jensen, 2013). Indeed, the number of in situ observations of moistening above 390 K is limited to only a few case studies, all quoted in the introduction. The lack of in situ evidence of moistening could be explained by i) overall lack of high-quality in situ observations of TTL water vapour; ii) logistical complexity of field operations in the regions of most vigorous convection (e.g. Central Africa, Amazonian region or Maritime continent) and iii) difficulty (or impossibility) of balloon and aircraft operations near convective storms.

450 In this study we report a new in situ evidence of convective hydration up to the 404 K level, detected as a 200—250 m thick enhancements of water vapour by up to 0.6 ppmv (18%). Such a petty feature can hardly be used to support the importance of convective hydration. However, as we point out above, these tiny enhancements owe their existence to very small convective cells with overshooting area of a few square kilometers only, remarkably smaller than other overshooting clouds observed on that day, whose cumulative effect on TTL water vapour may be substantial.

455 Interestingly, in our case the in-mixing from the extra-tropical stratosphere manifests itself in water vapour in a way very similar to what can be expected from convective hydration: the amplitude of enhancement in water vapour amounts to ~0.5 ppmv for both horizontal and vertical transport signatures. However the moistening effect of in-mixing on the tropical LS is limited by the small meridional gradient of water vapour and can hardly exceed 0.5-0.7 ppmv. In contrast to that, the convective hydration of LS, whose global effect is proportional to overshoot frequency and intensity, should be limited only by the temperature at the level of injection. This way, a relatively warm TTL/LS above the continents, hosting the most vigorous convection, provides favorable conditions for the convective hydration of LS.

465

470

Acknowledgements

This work and the TRO-pico project (<http://www.univ-reims.fr/site/autre/tro-pico/>) were supported by the French Agence Nationale de la Recherche (ANR) under contract ANR-2010-BLAN-609-01 (<http://www.univ-reims.fr/site/autre/tro-pico/>). We express our sincere gratitude to the personnel of IPMet for providing an infrastructure and manpower and especially for their invaluable help with balloon operation during the campaign. The following 475 satellite data used in this study are publically available: CALIPSO, https://eosweb.larc.nasa.gov/project/calipso/calipso_table; MLS, http://mls.jpl.nasa.gov/products/h2o_product.php; COSMIC, <http://cdaac-www.cosmic.ucar.edu/cdaac/>

480

485

490

495

500 **References**

- Anthes, R. A., Bernhardt, P. A., Chen, Y., Cucurull, L., Dymond, K. F., Ector, D., Healy, S. B., Ho, S.-P., Hunt, D. C., Kuo, Y.-H., Liu, H., Manning, K., McCormick, C., Meehan, T. K., Randel, W. J., Rocken, C., Schreiner, W. S., Sokolovskiy, S. V., Syndergaard, S., Thompson, D. C., Trenberth, K. E., Wee, T.-K., Yen, N. L., and Zeng, Z.: The COSMIC/FORMOSAT-3 Mission: Early Results, *B. Am. Meteorol. Soc.*, 89, 313–333, doi:10.1175/BAMS-89-3-313, 2008.
- 505 Bergman, J. W., Jensen, E. J., Pfister, L. & Yang, Q. Seasonal differences of vertical-transport efficiency in the tropical tropopause layer: On the interplay between tropical deep convection, large-scale vertical ascent, and horizontal circulations. *J. Geophys. Res.* 117, D05302, 2012.
- 510 Brabec, M., Wienhold, F. G., Luo, B. P., Vömel, H., Immler, F., Steiner, P., Hausammann, E., Weers, U., and Peter, T.: Particle backscatter and relative humidity measured across cirrus clouds and comparison with microphysical cirrus modelling, *Atmos. Chem. Phys.*, 12, 9135–9148, doi:10.5194/acp-12-9135-2012, 2012.
- Bukowiecki, N., Zieger, P., Weingartner, E., Jurányi, Z., Gysel, M., Neiningner, B., Schneider, B., Hueglin, C., Ulrich, A., Wichser, A., Henne, S., Brunner, D., Kaegi, R., Schwikowski, M., Tobler, L., Wienhold, F. G., Engel, I., Buchmann, B., Peter, T., and Baltensperger, U.: Ground-based and airborne in-situ measurements of the Eyjafjallajökull volcanic aerosol plume in Switzerland in spring 2010, *Atmos. Chem. Phys.*, 11, 10011-10030, doi:10.5194/acp-11-10011-2011, 2011.
- 515 Carminati, F., Ricaud, P., Pommereau, J.-P., Rivière, E., Khaykin, S., Attié, J.-L., and Warner, J.: Impact of tropical land convection on the water vapour budget in the tropical tropopause layer, *Atmos. Chem. Phys.*, 14, 6195-6211, doi:10.5194/acp-14-6195-2014, 2014.
- 520 Cirisan, A., Luo, B. P., Engel, I., Wienhold, F. G., Sprenger, M., Krieger, U. K., Weers, U., Romanens, G., Levrat, G., Jeannot, P., Ruffieux, D., Philipona, R., Calpini, B., Spichtinger, P., and Peter, T.: Balloon-borne match measurements of midlatitude cirrus clouds, *Atmos. Chem. Phys.*, 14, 7341-7365, doi:10.5194/acp-14-7341-2014, 2014.
- Chaboureaud, J.-P., Cammas, J.-P., Duron, J., Mascart, P. J., Sitnikov, N. M., and Voessing, H.-J.: A numerical study of tropical cross-tropopause transport by convective overshoots, *Atmos. Chem. Phys.*, 7, 1731-1740, doi:10.5194/acp-7-1731-2007, 2007.
- 525 Chemel, C., Russo, M. R., Pyle, J. A., Sokhi, R. S., and Schiller, C.: Quantifying the imprint of a severe Hector thunderstorm during ACTIVE/SCOUT-O3 onto the water content in the upper troposphere/lower stratosphere, *Mon. Weather Rev.*, 137, 2493–2514, doi:10.1175/2008MWR2666.1, 2009.
- 530 Corti, T., Luo, B. P., de Reus, M., Brunner, D., Cairo, F., Mahoney, M. J., Martucci, G., Matthey, R., Mitev, V., dos Santos, F. H., Schiller, C., Shur, G., Sitnikov, N. M., Spelten, N., Vossing, H. J., Borrmann, S., and Peter, T.: Unprecedented evidence for deep convection hydrating the tropical stratosphere, *Geophys. Res. Lett.*, 35, L10810, doi:10.1029/2008GL03641, 2008.
- Danielsen E.F.: In situ evidence of rapid, vertical, irreversible transport of lower tropospheric air into the lower stratosphere by convective cloud turrets and by large scale up welling in tropical cyclones, *J. Geophys. Res.*, 98, 8665-8681, 1993.
- 535 Dee, D. P., Uppala, S. M., Simmons, A. J., Berrisford, P., Poli, P., Kobayashi, S., Andrae, U., Balmaseda, M. A., Balsamo, G., Bauer, P., Bechtold, P., Beljaars, A. C. M., van de Berg, L., Bidlot, J., Bormann, N., Delsol, C., Dragani, R., Fuentes, M., Geer, A. J., Haimberger, L., Healy, S. B., Hersbach, H., Holm, E. V., Isaksen, I., Kallberg, P., Kohler, M., Matricardi, M., McNally, A. P., Monge-Sanz, B. M., Morcrette, J.-J., Park, B.-K., Peubey, C., de Rosnay, P., Tavolato, C., Thepaut, J.-N., and Vitart, F.: The ERA-Interim reanalysis: configuration and performance of the data assimilation system, *Q. J. R. Meteorol. Soc.*, 137, 553–597, doi:10.1002/qj.828, 2011.
- de Reus, M., Borrmann, S., Bansemmer, A., Heymsfield, A. J., Weigel, R., Schiller, C., Mitev, V., Frey, W., Kunkel, D., Kurten, A., Curtius, J., Sitnikov, N. M., Ulanovsky, A., and Ravegnani, F.: Evidence for ice particles in the tropical stratosphere from in-situ measurements, *Atmos. Chem. Phys.*, 9, 6775–6792, doi:10.5194/acp-9-6775-2009, 2009.
- 540 Durry, G., Amarouche, N., Joly, L., Liu, X., Parvitte, B., and Zeninari, V.: Laser diode spectroscopy of H₂O at 2.63 μm for atmospheric applications, *Appl. Phys. B*, 90, 573–580, 2008.
- Fueglistaler, S., Dessler, A.E., Dunkerton, T.J., Folkins, I., Fu, Q., Mote, P.W.: The tropical tropopause layer, *Rev. Geophys.*, 47, RG1004, doi:10.1029/2008RG000267, 2009.
- 550 Gattelman, A. and Forster, P. M.: A climatology of the tropical tropopause layer, *J. Meteorol. Soc. Japan*, 80, 911–924, 2002.
- Ghysels, M., Gomez, L., Cousin, J., Amarouche, N., Jost, H., and Durry, G.: Spectroscopy of CH₄ with a Difference Frequency Generation laser at 3.3 micron for atmospheric applications, *Appl. Phys. B*, 104, 989-1000, 2011.
- 555 Ghysels, M., Gomez, L., Cousin, J., Tran, H., and Durry, G.: Temperature dependence of air-broadening, air-narrowing and line-mixing coefficients of the methane (R(6), v₃) manifold for atmospheric applications, *J. Quant. Spectrosc. Ra.*, 133, 206-216, 2014.
- Ghysels, M., Riviere, E. D., Khaykin, S., Stoeffler, C., Amarouche, N., Pommereau, J.-P., Held, G., and Durry, G.: Intercomparison of in situ water vapor balloon-borne measurements from Pico-SDLA H₂O and FLASH-B in the tropical UTLS, *Atmos. Meas. Tech.*, 9, 1207-1219, doi:10.5194/amt-9-1207-2016, 2016.
- 560 Grosvenor, D. P., Choularton, T. W., Coe, H., and Held, G.: A study of the effect of overshooting deep convection on the water content of the TTL and lower stratosphere from Cloud Resolving Model simulations, *Atmos. Chem. Phys.*, 7, 4977-5002, doi:10.5194/acp-7-4977-2007, 2007.



- Holton, J. R. and Gettelman, A.: Horizontal transport and the dehydration of the stratosphere, *Geophys. Res. Lett.*, 28, 2799–2802, 2001.
- 565 Homan, C. D., Volk, C. M., Kuhn, A. C., Werner, A., Baehr, J., Viciani, S., Ulanovski, A., and Ravegnani, F.: Tracer measurements in the tropical tropopause layer during the AMMA/SCOUT-O3 aircraft campaign, *Atmos. Chem. Phys.*, 10, 3615–3627, doi:10.5194/acp-10-3615-2010, 2010.
- Iwasaki, S., Shibata, T., Nakamoto, J., Okamoto, H., Ishimoto, H., and Kubota, H.: Characteristics of deep convection measured by using the A-train constellation, *J. Geophys. Res.*, 115, D06207, doi:10.1029/2009JD013000, 2010.
- 570 Jensen, E. J., Ackerman, A. S., Smith J. A.: Can overshooting convection dehydrate the tropical tropopause layer?, *J. Geophys. Res.*, 112, D11209, doi:10.1029/2006JD007943, 2007.
- Kelly, K. K., Proffitt, M. H., Chan, K. R., Loewenstein, M., Podolske, J. R., Strahan, S. E., Wilson, J. C., and Kley, D.: Water vapour and cloud water measurements over Darwin during the STEP 1987 tropical mission, *J. Geophys. Res.*, 98, 8713–8723, 1993.
- 575 Khaykin, S., Pommereau, J.-P., Korshunov, L., Yushkov, V., Nielsen, J., Larsen, N., Christensen, T., Garnier, A., Lukyanov, A., and Williams, E.: Hydration of the lower stratosphere by ice crystal geysers over land convective systems, *Atmos. Chem. Phys.*, 9, 2275–2287, doi:10.5194/acp-9-2275-2009, 2009.
- Khaykin, S. M., Pommereau, J.-P., and Hauchecorne, A.: Impact of land convection on temperature diurnal variation in the tropical lower stratosphere inferred from COSMIC GPS radio occultations, *Atmos. Chem. Phys.*, 13, 6391–6402, doi:10.5194/acp-13-6391-2013, 2013a.
- 580 Khaykin, S. M., Engel, I., Vömel, H., Formanyuk, I. M., Kivi, R., Korshunov, L. I., Krämer, M., Lykov, A. D., Meier, S., Naebert, T., Pitts, M. C., Santee, M. L., Spelten, N., Wienhold, F. G., Yushkov, V. A., and Peter, T.: Arctic stratospheric dehydration – Part 1: Unprecedented observation of vertical redistribution of water, *Atmos. Chem. Phys.*, 13, 11503–11517, doi:10.5194/acp-13-11503-2013, 2013b.
- 585 Konopka, P., Groöß, J.-U., Ploeger, F., and Müller, R.: Annual cycle of horizontal in-mixing into the lower tropical stratosphere, *J. Geophys. Res.*, 114, D19111, doi:10.1029/2009JD011955, 2009.
- Konopka, P., Groöß, J.-U., Günther, G., Ploeger, F., Pommrich, R., Müller, R., and Livesey, N.: Annual cycle of ozone at and above the tropical tropopause: observations versus simulations with the Chemical Lagrangian Model of the Stratosphere (CLaMS), *Atmos. Chem. Phys.*, 10, 121–132, doi:10.5194/acp-10-121-2010, 2010.
- 590 Liu, C. and Zipser, E.J.: Global distribution of convection penetrating the tropical tropopause, *J. Geophys. Res.*, doi:10.1029/2005JD006063, 2005.
- Liu, X. M., Rivière, E. D., Marécal, V., Durrý, G., Hamdouni, A., Arteta, J., and Khaykin, S.: Stratospheric water vapour budget and convection overshooting the tropopause: modelling study from SCOUT-AMMA, *Atmos. Chem. Phys.*, 10, 8267–8286, doi:10.5194/acp-10-8267-2010, 2010.
- 595 Marcy T. P., Popp, P. J., Gao, R. S., Fahey, D. W., Ray, E. A., Richard, E. C., Thompson, T. L., Atlas, E. L., Loewenstein, M., Wofsy, S. C., Park, S., Weinstock, E. M., Swartz, W. H., and Mahoney, M. J.: Measurements of trace gases in the tropical tropopause layer, *Atmos. Environ.*, 41, 7253–7261, doi:10.1016/j.atmosenv.2007.05.032, 2007.
- 600 Massie, S. T., Gille, J., Craig, C., Khosravi, R., Barnett, J., Read, W., and Winker, D.: HIRDLS and CALIPSO observations of tropical cirrus, *J. Geophys. Res.*, 115, D00H11, doi:10.1029/2009JD012100, 2010.
- McKenna, D. S., Groöß, J.-U., Günther, G., Konopka, P., Müller, R., Carver, G., and Sasano, Y.: A new Chemical Lagrangian Model of the Stratosphere (CLaMS): 2. Formulation of chemistry scheme and initialization, *J. Geophys. Res.*, 107, 4256, doi:10.1029/2000JD000113, 2002.
- 605 Nielsen, J.K., Larsen, N., Cairo, F., Di Donfrancesco, G., Rosen, J.M., Durrý, G., Held, G. and Pommereau, J.-P.: Solid particles in the tropical lower stratosphere, *Atm. Chem. Phys.*, 7, 685–695, 2007.
- Ploeger, F., Konopka, P., Müller, R., Fueglistaler, S., Schmidt, T., Manners, J. C., Groöß, J.-U., Günther, G., Forster, P. M., and Riese, M.: Horizontal transport affecting trace gas seasonality in the Tropical Tropopause Layer TTL, *J. Geophys. Res.*, 117, 09303, doi:10.1029/2011JD017267, 2012.
- 610 Pommrich, R., Müller, R., Groöß, J.-U., Konopka, P., Ploeger, F., Vogel, B., Tao, M., Hoppe, C. M., Günther, G., Spelten, N., Hoffmann, L., Pumphrey, H.-C., Viciani, S., D’Amato, F., Volk, C. M., Hoor, P., Schlager, H., and Riese, M.: Tropical troposphere to stratosphere transport of carbon monoxide and long-lived trace species in the Chemical Lagrangian Model of the Stratosphere (CLaMS), *Geosci. 20 Model Dev.*, 7, 2895–2916, doi:10.5194/gmd-7-2895-2014, <http://www.geosci-model-dev.net/7/2895/2014/>, 2014.
- Randel, W. J. and Jensen, E. J.: Physical processes in the tropical tropopause layer and their roles in a changing climate, *Nat. Geosci.*, 6, 196–176, 2013.
- 615 Randel, W. J., Zhang, K., and Fu, R.: What controls stratospheric water vapor in the NH summer monsoon regions?, *J. Geophys. Res.-Atmos.*, 120, 7988–8001, doi:10.1002/2015JD023622, 2015.
- Ricaud, P., Barret, B., Attié, J.-L., Motte, E., Le Flochmoën, E., Peuch, V.-H., Livesey, N., Lambert, A., and Pommereau, J.-P.: Impact of land convection on troposphere-stratosphere exchange in the tropics, *Atmos. Chem. Phys.*, 7, 5639–5657, doi:10.5194/acp-7-5639-2007, 2007.
- 620 Ricaud, P., Pommereau, J.-P., Attié, J.-L., Le Flochmoën, E., El Amraoui, L., Teyssède, H., Peuch, V.-H., Feng, W., and Chipperfield, M. P.: Equatorial transport as diagnosed from nitrous oxide variability, *Atmos. Chem. Phys.*, 9, 8173–8188, doi:10.5194/acp-9-8173-2009, 2009.
- Sargent, M. R., Smith, J. B., Sayres D. S., and Anderson J. G.: The roles of deep convection and extratropical mixing in the tropical tropopause layer: An in situ measurement perspective, *J. Geophys. Res. Atmos.*, 119, 12,355–
- 625



12,371, doi:10.1002/2014JD022157, 2014.

Schiller, C., Grooß, J.-U., Konopka, P., Plöger, F., Silva dos Santos, F. H., and Spelten, N.: Hydration and dehydration at the tropical tropopause, *Atmos. Chem. Phys.*, 9, 9647-9660, doi:10.5194/acp-9-9647-2009, 2009.

630 Solomon, S., Rosenlof, K. H., Portmann, R.W., Daniel, J. S., Davis, S. M., Sanford, T. J., and Plattner, G. K., Contributions of stratospheric water vapor to decadal changes in the rate of global warming, *Science*, 327, 1219–1223, 2010.

Stein, A.F., Draxler, R.R., Rolph, G.D., Stunder, B.J.B., Cohen, M.D., and Ngan, F.: NOAA's HYSPLIT atmospheric transport and dispersion modeling system, *Bull. Amer. Meteor. Soc.*, 96, 2059-2077, <http://dx.doi.org/10.1175/BAMS-D-14-00110.1>, 2015.

635 Vernier, J.-P., Pommereau, J.-P., Thomason, L. W., Pelon, J., Garnier, A., Deshler, T., Jumelet, J., and Nielsen, J. K.: Overshooting of clean tropospheric air in the tropical lower stratosphere as seen by the CALIPSO lidar, *Atmos. Chem. Phys.*, 11, 9683-9696, doi:10.5194/acp-11-9683-2011, 2011.

640 Vernier, J.-P., Fairlie, T. D., Natarajan, M., Wienhold, F. G., Bian, J., Martinsson, B. G., Crumeyrolle, S., Thomason, L. W., and Bedka, K.: Increase in upper tropospheric and lower stratospheric aerosol levels and its potential connection with Asian Pollution, *J. Geophys. Res.-Atmos.*, 120, 1608–1619, doi:10.1002/2014JD022372, 2015.

Yushkov, V., Astakhov V., and Merkulov, S.: Optical balloon hygrometer for upper-troposphere and stratosphere water vapor measurements, in: *Proceedings SPIE 3501, Optical Remote Sensing of the Atmosphere and Clouds*, Beijing, China, 14 September 1998, 439–445, 1998.

645

650

655

660

665

670

675

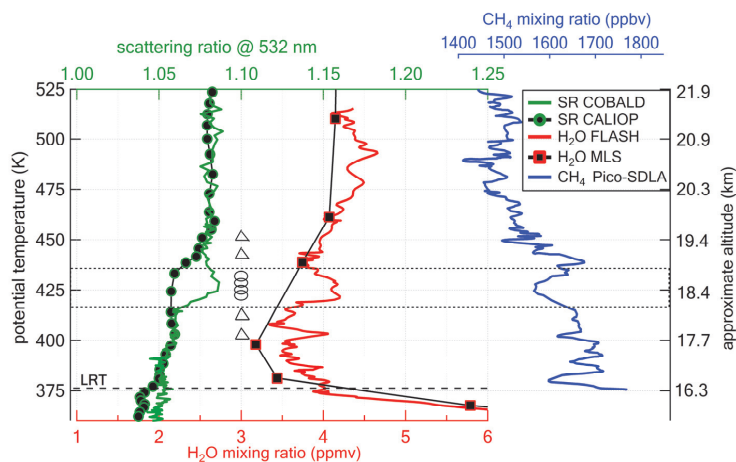


Figure 1. Vertical profiles of scattering ratio from COBALD (13 March) and CALIPSO (February zonal-mean), water vapour from FLASH-B (13 March) and MLS (13 March), methane (Pico-SDLA on 14 March). Horizontal dotted lines mark the lower and upper boundaries of the water/aerosol-enriched and methane-depleted layer. Horizontal dashed line marks the Lapse Rate Tropopause (LRT) level. The circles and triangles indicate the altitude levels, from where CLaMS back trajectories were initialized (same convection for the markers is used in Fig. 2). See text for detail.

680

685

690

695

700

705

710

715

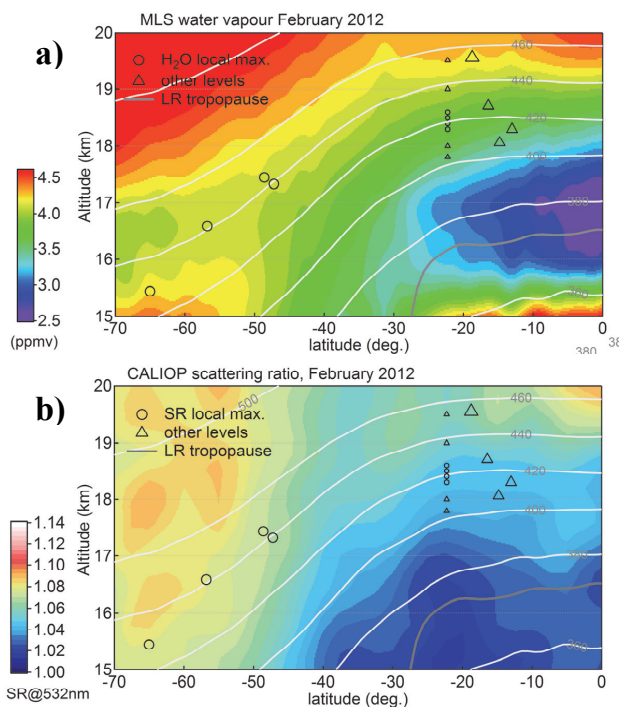


Figure 2. Latitude-altitude section of monthly/zonal mean MLS water vapour (a) and CALIPSO scattering ratio (b). Larger markers (circles and triangles) indicate the location of the sampled air masses 15 days prior to balloon sounding on 13 March (same convention as in Fig.1) Smaller markers indicate the locations where trajectories were initialized. Circles denote the trajectories initialized from the WV/SR enhancement; triangles denote trajectories initialized at levels below and above. The isentropes (white contours) and the Lapse Rate (LR) tropopause (grey curve) were calculated using zonally-averaged COSMIC GPS radio-occultation measurements (Anthes et al., 2008).

720

725

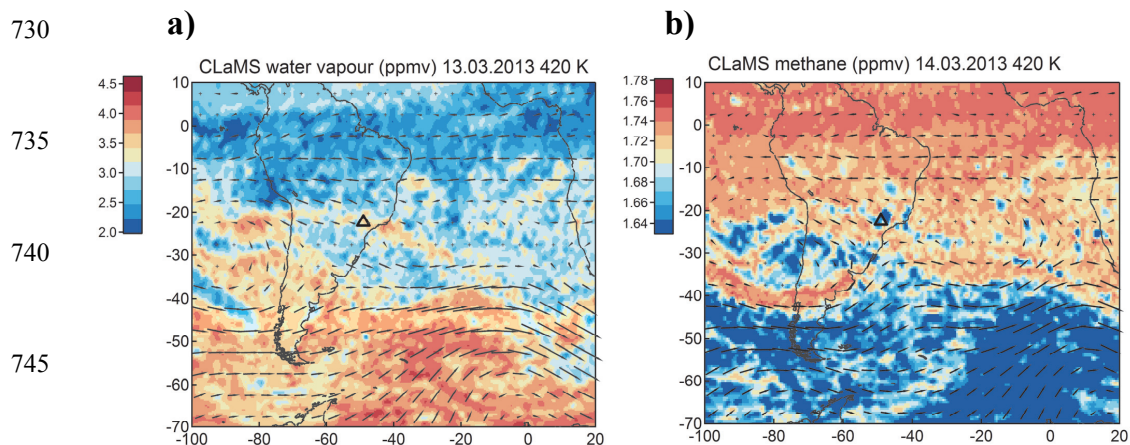


Figure 3. CLaMS simulated fields of water vapour for 13 March (a) and methane for 14 March (b) with ERA-Int winds superimposed. A filament of water-rich and methane-poor air extending above the sounding location (marked by the triangle) is clearly visible.

755

760

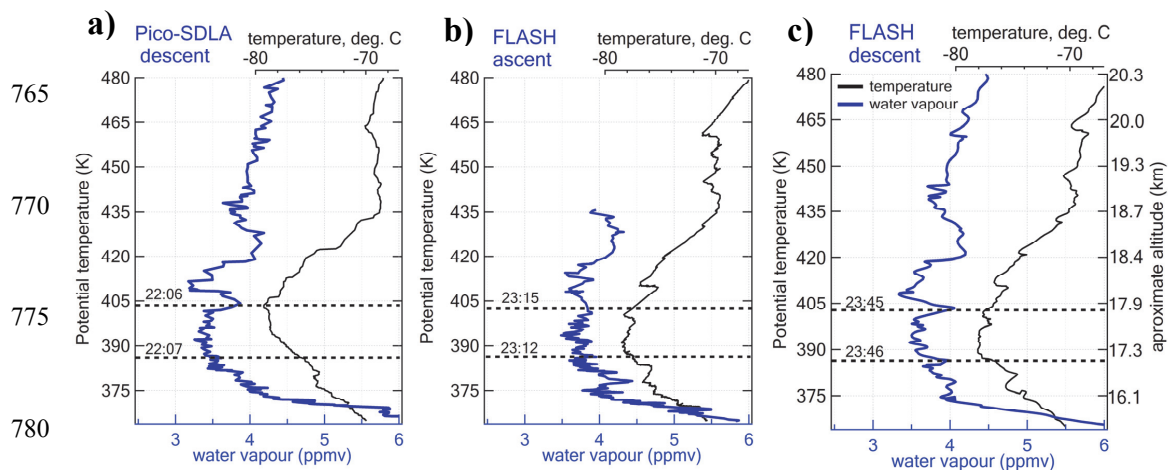
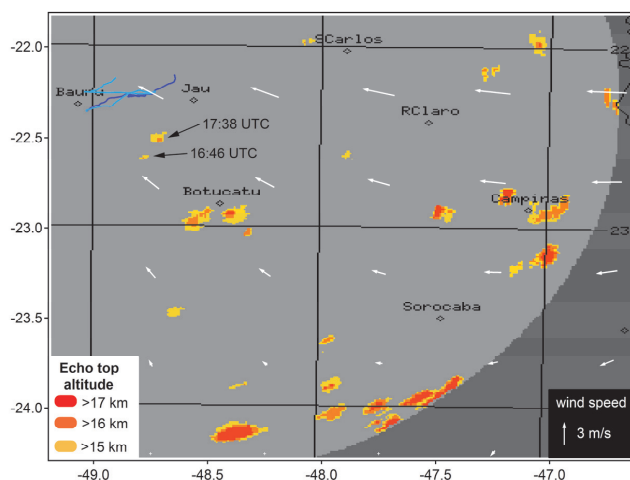


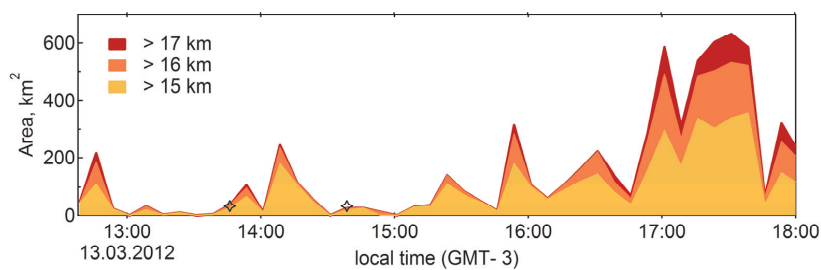
Figure 4. Water vapour (blue) and temperature (black) vertical profiles obtained successively in time on 13 March by (a) Pico-SDLA on descent, (b) FLASH-B on ascent (outgassing-biased part removed), (c) FLASH-B on descent. The dashed lines mark the levels, where hydrated layers in (c) were sampled with indication of the sampling time.

785



790 **Figure 5. Composite radar image of all convective cells reaching above 15 km detected on 13 March by IPMet radar in the upwind quadrant of Bauru. Black arrows indicate the overshooting cells potentially responsible for the hydrated layers shown in Fig. 4. White arrows represent the mean wind field between 100 and 70 hPa from ERA-Int reanalysis (18 h UT). Blue lines indicate the balloon trajectories (FLASH-B dark blue, Pico-SDLA light blue).**

795



800

Figure 6. Temporal evolution of cumulative overshooting area at different levels of TTL recorded by IPMet radar on 13 March within its 240 km range (10 dBZ reflectivity threshold). The black stars mark the timing of overshooting cells shown in Fig. 6.

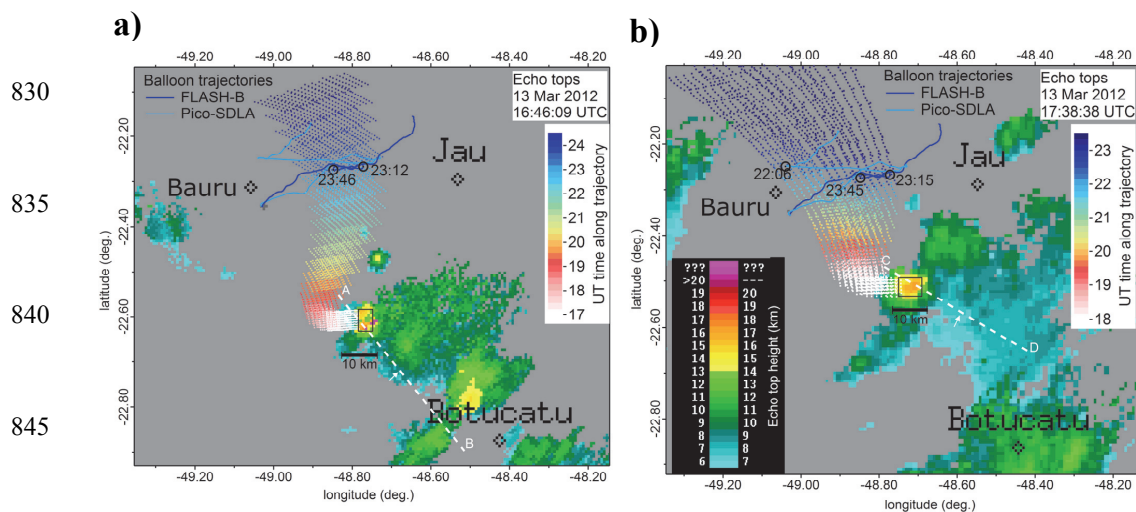
805

810

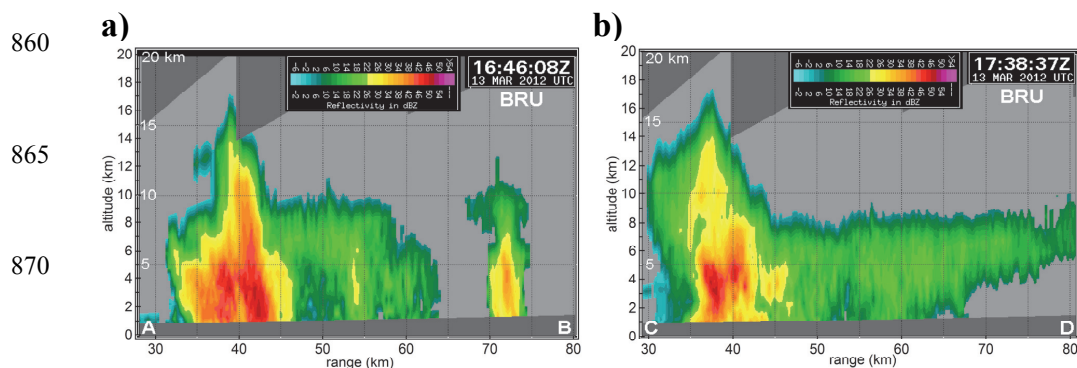
815

820

825



850 **Figure 7.** Echo top maps (reflectivity threshold 10 dBZ) recorded by IPMet radar on 13 March. The overshooting cells,
 linked by trajectories with hydrated layers at 386 K and 404 K are outlined by rectangles in (a) and (b) respectively. Solid
 lines indicate the trajectories of balloons carrying FLASH-B and Pico-SDLA hygrometers with indication of time (UT) when
 386 K and 404 K levels were sampled. Dots depict the ensembles of forward trajectories (color-coded by UT) initialized within
 855 the rectangle. Dashed white lines A-B in (a) and C-D (b) show the bases of vertical cross-section of the convective cells
 provided in Fig. 8.



875 **Figure 8.** Vertical cross section of IPMet radar reflectivity on 13 March of: (a) Cell 1 (16:46 UT, baseline A-B in Fig 7a),
 (b) Cell 2 (17:38 UT, baseline C-D in Fig 7b). Dark grey shading in the top of the plots corresponds to the areas without radar
 PPI overlapping coverage.